Hysteretic Effects in Droplet Motions on Heterogeneous Substrates: Direct Numerical Simulation

Leonard W. Schwartz

Departments of Mechanical Engineering and Mathematical Sciences, The University of Delaware, Newark, Delaware 19716

Received December 22, 1997. In Final Form: April 1, 1998

A method of calculation is introduced that allows the simulation of the time-dependent three-dimensional motion of liquid droplets on solid substrates for systems with finite equilibrium contact angles. The contact angle is a prescribed function of position on the substrate. An evolution equation is given, using the lubrication assumption, that includes viscous, capillary, and disjoining forces. Motion to and from dry substrate regions is made possible by use of a thin energetically stable wetting layer. We simulate motion on heterogeneous substrates with periodic arrays of high-contact-angle patches. For a homogeneous substrate, calculated droplet spreading rates are compared to published experimental results, revealing the need for a time-scale correction. Two different problems are treated. The first is spontaneous motion driven only by wetting forces. If the contact-angle difference is sufficiently high, the droplet can find several different stable positions, depending on the previous history of the motion. A second simulation treats a forced cyclical motion. Energy dissipation per cycle for a heterogeneous substrate is found to be larger than that for a uniform substrate with the same total energy. Comparison is made with simple quasi-static theories.

1. Introduction

Wetting and capillary considerations during the slow motion of liquids on solid substrates are important in both the technological and natural worlds. Applications include the spreading behavior of liquid coatings, as well as flows in oil reservoirs, chemical reactors, and heat exchangers. Some biological application areas are motions in the tear film on the cornea of the eye, flows on liquid-covered membranes in the lungs, and the general area of cell motility, where cell motions have many of the features of inert liquid droplets.[1] The spreading properties of agrochemicals such as pesticides and insecticides are important determinants of their effectiveness. Capillary forces are often dominant in problems of small physical dimensions; however, they can also be important for large-scale phenomena when body forces are very weak, as in the microgravity environment of orbiting satellites in space, for example.

Most substrates are of intermediate energy in that a liquid droplet, when placed upon them, ultimately achieves a static shape with a nonzero value of contact angle. Systems exhibiting nonzero contact angles are also termed "partially wetting". The contact angle is the angle, measured within the liquid, at the so-called wetting or contact line where the three phases, solid (S), liquid (L), and vapor (V), meet. The Young−Laplace equation, derived using either force or energy considerations, predicts a unique value for the contact angle as a function of the three pairwise interfacial energies γ_{SL}, γ_{SV}, and γ_{LV}. The latter is often termed the surface tension, or surface energy density σ. The equation is

$$\gamma_{SL} + \sigma \cos \theta_e = \gamma_{SV} \tag{1.1}$$

There are serious experimental difficulties in measuring a single reproducible value of equilibrium contact angle θ_e in particular systems, and often two different values are measured, depending on whether the liquid has recently advanced onto a previously dry substrate or recently receded, leaving behind a sensibly dry substrate. These angles are termed the advancing contact angle θ_a and the receding angle θ_r. Systems for which θ_a and θ_r are different are said to display contact angle hysteresis (CAH). Invariably the receding angle is smaller than the advancing one.

Contact angle hysteresis has been attributed to the chemical nonhomogeniety of the substrate and the possibility that the liquid front may be trapped in different configurations, each configuration corresponding to a local minimum of the total free energy of the system. Often the scale of substrate heterogeneity is much smaller than macroscopic measurements can discern. The problem may be simplified by assuming that a single parameter characterizes the geometry of the system. For example, Johnson and Dettre[2] consider an axisymmetric sessile drop that is placed at the center of a patterned substrate composed of alternating concentric rings of different materials. The equilibrium contact angle takes on a different constant value on each material. Their analysis looked for local minima in the functional describing the free energy of the system. For given values of drop volume, ring width, and contact angles, they found a range of drop radii over which the free energy versus radius curve has a set of local minima. Assuming that the drop moves very slowly, its edge may be trapped at the first local energy minimum that is encountered. Although the scale of the heterogeneity, in this case the ring width, may be small, the range of energy minima, termed the metastable range, may be much larger, leading to quite large values of CAH. Similar calculations were performed by Neumann and Good[3] for horizontal stripes of different materials applied to a plate that is held vertically in a reservoir of liquid. If the contact line is also assumed to be horizontal, a metastable energy range and correspondingly different values of advancing and receding angle can be predicted,

(1) Greenspan, H. P. *J. Fluid Mech.* **1978**, *84*, 125−143.

(2) Johnson, R. E.; Dettre, R. H. *J. Phys. Chem.* **1964**, *68*, 1744.

(3) Neumann, A. W.; Good, R. J. *J. Colloid Interface Sci.* **1972**, *38*, 341.

S0743-7463(97)01407-8 CCC: $15.00 © 1998 American Chemical Society
Published on Web 06/09/1998

depending on whether the plate is moved into or out of the liquid bath. The analysis included gravitational potential energy in the free energy of the system. Physical roughness is believed to play a role similar to that of chemical heterogeneity. Dussan[4] demonstrates that patterns of alternating surface inclination on a chemically homogeneous substrate may lead to different "apparent" values of contact angle.

The assumption that the contact line shape is known a priori is highly restrictive. Schwartz and Garoff[5] considered the vertical plate geometry with horizontal wettability stripes and allowed the contact line shape to be found as part of the energy minimization procedure. They found that straight three-phase lines correspond to the minimum energy solutions only in special circumstances. As the fluid advances and recedes along the substrate, the contact line alternates between straight and nonrectilinear configurations. The extra freedom allowed to the system leads to a dramatic lowering of the heights of the energy barriers. The metastable range is considerably reduced, as is the degree of CAH. Waves moving transversely to the direction of plate motion were predicted by the analysis when the contact line was near a wettability boundary. These waves were then observed experimentally using a silvered plate whose lower half was coated with a surfactant monolayer. In later work[6] more general patterns of wettability were considered, also for the problem of capillary rise onto a partially submerged vertical plate. It was found that CAH was a strong function of the details of the "patch" pattern. Predictions of the progression of the three-phase line as it transverses the wettability pattern include alternating continuous deformations and discrete jumps to other solution families. The phrase "sticking, stretching, and jumping" was introduced to describe these motions.

Missing in the above analyses is any consideration of dynamic effects. Even on a perfectly homogeneous surface, apparent contact angles while a liquid is advancing are different from the apparent angles when the liquid recedes. These so-called dynamic contact angles are not accessible to the previous quasi-static formulations. One must also distinguish between spontaneous and forced motions. Spontaneous motions are those driven solely by the energy difference between a given nonequilibrium configuration and a final statically stable configuration. The quasi-static analyses can give no indication of the time scales in spontaneous motion. Spreading of a drop on a plate is an example of such a spontaneous motion. The response of a liquid to the motion of a vertical plate, as discussed above, is an example of a forced motion. While the time scale is set, in such cases as the period of an imposed oscillation, the quasi-static theories require that the motion be so slow that the system has time to relax to a stable equilibrium configuration at each instant. This certainly need not be the case. Also the energy balance for the quasi-static theories is incomplete. There is no consideration of dissipative viscous effects which, even for slow motions, can be comparable to changes in the free energy of the system. A principal purpose of the present paper is to resolve these inadequacies by formulating and solving a mathematical model for the direct time-dependent numerical simulation of either forced or spontaneous spreading of a liquid droplet on a mixed-wettable surface. Hysteretic effects will be explored. These include contact-angle hysteresis, as defined above, as well as hysteresis in the traditional physical sense. Traditional hysteresis here refers to the energy dissipated per cycle in a forced periodic motion. This energy loss is approximately proportional to the speed of an imposed motion and is present even for an ideally homogeneous substrate.

The following section discusses the mathematical model for droplet motion on a heterogeneous substrate. It is based on the long-wave or lubrication approximation for the unsteady motion of a liquid coating layer on a flat substrate. The approximation requires that the inclination of the liquid free surface, relative to the substrate, be small. Inertial effects are neglected; thus, a suitably defined Reynolds number must also be small. Systematic derivations of lubrication theory, as an expansion in the inclination of the free surface, are given by Benney[7] without surface tension and by Atherton and Homsy,[8] where surface tension is included. Because integration across the thin dimension is performed analytically, the dimensionality in space is reduced from three to two in the time-dependent numerical simulation. For a partially wetting system, the shape of statically stable liquid droplets can be represented mathematically using the Frumkin−Deryaguin model.[9−11] The substrate region near the margin of the macroscopic droplet is covered with a submicroscopic layer of wetting liquid. This wetting layer is maintained in a state of stable equilibrium through the action of intermolecular forces. There is excess or "disjoining" pressure in the thin film that arises from a variety of causes; these contributions are often divided into molecular, ionic-electrostatic, and structural components. A useful survey of the substantial theoretical and experimental literature on disjoining pressure is given by Mohanty.[12] In the contact region, the condition of constancy of total pressure, including capilllary and disjoining components, determines the shape of the liquid−vapor interface. The apparent contact angle, or maximum slope of the interface, may be found as a function of the surface tension and the parameters in the expression used for the disjoining pressure.

The existence of the wetting layer serves another purpose for dynamic simulations. The lubrication formulation, like the full Navier−Stokes problem from which it is derived, does not allow liquid motion to or from perfectly dry regions of the substrate. The difficulty lies in the incompatibility between the usual no-slip condition, where the moving liquid meets the substrate, and the boundary conditions on the liquid−vapor interface, leading to a nonintegrable force singularity where these two interfaces meet at the contact line.[13] The thin wetting layer alleviates this problem and is an alternative to the slip models otherwise used in dynamic studies.[1,14] Asymptotic analyses of spreading using a thin wetting layer are given by Tanner[15] and Tuck and Schwartz.[16] Experimental data for the speed of spreading drops in various systems suggests that the wetting layer thickness, h^* say, lies in the broad range 1−100 nm.[17−19] A number of dynamic studies, using various forms of the disjoining

(4) Dussan, V. E. B. *Annu. Rev. Fluid Mech.* **1979**, *11*, 371.
(5) Schwartz, L. W.; Garoff, S. *J. Colloid Interface Sci.* **1985**, *106*, 422.
(6) Schwartz, L. W.; Garoff, S. *Langmuir* **1985**, *1*, 219.
(7) Benney, D. J. *J. Math. Phys.* **1966**, *45*, 150.
(8) Atherton, R. W.; Homsy, G. M. *Chem. Eng. Commun.* **1976**, *2*, 57.
(9) Frumkin, A. N. *Zh. Fiz. Khim.* **1938**, *12*, 337.
(10) Derjaguin, B. V. *Zh. Fiz. Khim.* **1940**, *14*, 137.
(11) Churaev, N. V.; Sobolev, V. D. *Adv. Colloid Interface Sci.* **1995**, *61*, 1.
(12) Mohanty, K. K. Ph.D. Dissertation, University of Minnesota, 1981. See also: Sharma, A. *Langmuir* **1993**, *9*, 861.
(13) Huh, C.; Scriven, L. E. *J. Colloid Interface Sci.* **1971**, *35*, 85.
(14) Hocking, L. M. *Q. J. Mech. Appl. Math.* **1981**, *34*, 37.
(15) Tanner, L. *J. Phys. (D)* **1979**, *12*, 1473.
(16) Tuck, E. O.; Schwartz, L. W. *SIAM Rev.* **1990**, *32*, 453.
(17) Lelah, M. D.; Marmur, A. M. *J. Colloid Interface Sci.* **1981**, *82*, 518.

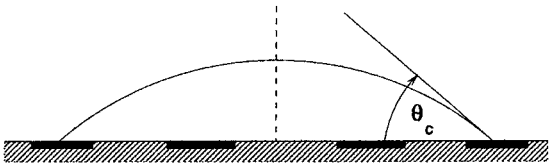

Figure 1. Schematic diagram of a liquid droplet on a mixed-wettable substrate.

pressure term in a one-dimensional or axisymmetric lubrication model for wetting/dewetting, have also appeared.[18,20−23] A fully two-dimensional spreading problem, with disjoining pressure effect, has recently been considered by us.[24] That paper treated the spontaneous motion of a droplet placed on a horizontal glass slide near the center of a "cross" of high-contact-angle material. The droplet ultimately splits into four unequal segments as the liquid withdraws onto the lower-contact-angle regions. The numerical simulation was compared with an experiment using glycerin as the spreading liquid and a Teflon cross. All qualitative features of the observed motion were reproduced by the simulation. However a time-scale correction needed to be applied due primarily to the too-large value of the wetting layer thickness used in the simulation.

Section 2 also considers the energetics of droplet spreading. The free energy of the system is taken to be the sum of the appropriate interfacial energy densities integrated over the instantaneous areas of the corresponding interfaces. Gravitational contributions are omitted here but could have been included without difficulty; thus, we consider only relatively small droplets. For the glycerin droplet treated previously,[24] the average radius R_0 on the substrate was about 4 mm. The corresponding Bond number $Bo = \rho g R_0^2/\sigma$ is 2.5, where ρ and g are the liquid density and the acceleration of gravity, respectively. We performed simulations with gravity effects both included and omitted. The differences were limited primarily to the speed of motion, with the predicted speed greater by about 5% when gravity is included. Thus for drops of this size or smaller, gravitational effects for a drop placed upon a horizontal substrate are relatively unimportant. For spontaneous motions, it is shown that the rate of decrease of the total free energy of the system is equal to the rate of viscous dissipation. For forced motions, on the other hand, the energy balance also must include the rate of working by liquid injection. Some details of the numerical procedure are given in subsection 2.2.

Sections 3 and 4 discuss calculations and results for droplet motion on substrates with discrete patches of high-contact-angle material or "grease". A schematic diagram is shown in Figure 1, where the blackened areas are the grease patches. Two different patch patterns, shown in Figure 2, are used in this study. They are both doubly periodic on the substrate. The pattern denoted "isolated spots" is a simple square array where the fractional coverage of grease is a small fraction of the total substrate area. The checkerboard pattern is a staggered array with

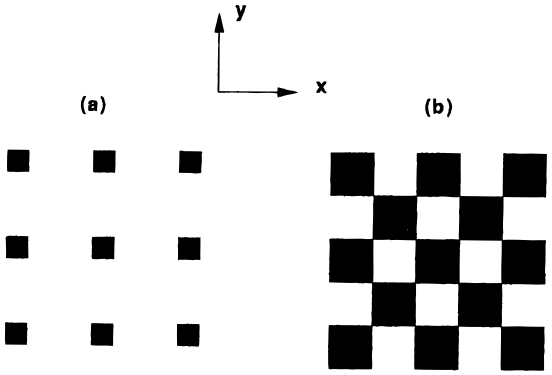

Figure 2. Substrate wettability patterns used in this study. The dark regions have larger values of contact angle than the surrounding field: (a) isolated spot pattern; (b) checkerboard pattern.

each of the two substrate materials occupying an equal fraction of the substrate. The mathematical procedure for generating these patterns is given in the Appendix.

For the isolated spot pattern, results are given for a number of simulations of spontaneous spreading. In each case, the substrate-average wettability is the same. Two different types of simulations are performed: ones where the droplet advances and others where the droplet recedes. In both cases the droplets eventually stabilize. By varying the wettability contrast, we establish the level of contrast necessary for hysteresis, that is when the final positions in advance and recede are not the same. For a particular case where CAH occurs, the detailed calculations are compared with the results of a simple theory that assumes the droplet shape is axisymmetric. While the simple model gives a good estimate of the final free energy, it does not predict any hysteresis. When the wettability contrast is not sufficiently great to cause different final positions, its influence is still felt. The time required to reach equilibrium is increased, in proportion to the degree of heterogeneity.

Results for forced spreading are given in section 4. A prototypical experiment is simulated where the liquid drop is forced to expand and then retract by cyclical pumping through a hole in the substrate lying underneath the drop. The cycle time is varied, and the total work per cycle is calculated. The viscous losses for a uniform substrate are approximately inversely proportional to the cycle time. The additional dissipations on a patterned substrate are relatively insensitive to speed. Both the checkerboard and isolated-spot patterns are used in this section. While the isolated spots are more effective for "pinning" the contact line, the checkerboard, using a smaller wettability contrast, can dissipate more energy. The results suggest that a wettability pattern may be optimized to satisfy a particular purpose.

Further remarks are given in the final section. The need for additional theoretical and experimental work to address unexplored areas is explained. Implications for terrestrial and microgravity applications are also discussed.

2. Mathematical Model

We consider a layer of liquid, or an isolated droplet, on a plane substrate. x, y, and z form a right-handed triad with the x and y axes lying on the substrate. The liquid surface corresponds to $z = h(x,y,t)$ where t is time. The statement of mass conservation is

$$h_t = -\nabla\cdot\mathbf{Q} + w_i(x,y,t) \qquad (2.1)$$

(18) Teletzke, G.; Davis, H. T.; Scriven, L. E. *Chem. Eng. Comm.* **1987**, *55*, 41.
(19) Starov, V. M.; Kalinin, V. V.; Chen, J.-D. *Adv. Colloid Interface Sci.* **1994**, *50*, 187.
(20) Williams, M. B.; Davis, S. H. *J. Colloid Interface Sci.* **1982**, *90*, 220.
(21) Kheshgi, H. S.; Scriven, L. E. *Chem. Eng. Sci.* **1991**, *46*, 519.
(22) Mitlin, V. S.; Petviashvili, N. V. *Phys. Lett. A* **1994**, *192*, 323.
(23) Jameel, A. T.; Sharma, A. *J. Colloid Interface Sci.* **1994**, *164*, 416.
(24) Schwartz, L. W.; Eley, R. R. *J. Colloid Interface Sci.*, in press.

Here **Q** is the two-dimensional areal flux vector defined as

$$\mathbf{Q} = \int_0^{h(x,y)} (u,v)\, \mathrm{d}z$$

where u and v are velocity components in the x and y directions, respectively. Likewise ∇ is a two-dimensional operator with respect to x and y. w_i is a local injection rate that is an input function of substrate position and time. It will be used for the forced-motion simulations in section 4.

Under the assumptions of lubrication theory, that is, the motion is sufficiently slow that inertial forces may be neglected and that the free surface is inclined at a small angle relative to the substrate, the momentum equation for an assumed Newtonian liquid may be integrated to yield

$$Q = -\frac{1}{3\mu}(h^3 \nabla p) \tag{2.2}$$

Here μ is the viscosity and the pressure p is independent of z. The no-slip condition for the velocity has been applied on the substrate, and the liquid free surface is stress-free. The pressure in the liquid is given by

$$p = -\sigma\kappa - \Pi \approx -\sigma\nabla^2 h - \Pi \tag{2.3}$$

and the pressure above the liquid is taken to be zero without loss of generality. The first term on the right is an approximation of the free-surface curvature κ when the surface slope is small. The error in this curvature approximation is proportional to the square of the surface inclination. σ is surface tension, and the so-called disjoining pressure is given by the two-term model

$$\Pi = B\left[\left(\frac{h^*}{h}\right)^n - \left(\frac{h^*}{h}\right)^m\right] \tag{2.4}$$

B and the exponents n and m are positive constants with $n > m > 1$. The local disjoining energy density

$$e^{(d)}(h) = -\int_{h^*}^{h} \Pi(h')\, \mathrm{d}h' \tag{2.5}$$

has a single stable energy minimum at the thin wetting-layer thickness $h = h^*$. Because the disjoining pressure is assumed to depend only on the local interfacial separation h, the validity of expressions such as eq 2.4 also requires the small-slope approximation.

A diagram of the edge of a drop at static equilibrium is shown in Figure 3. It is useful to review the basic force balance and its relationship to the equivalent line tensions using the present disjoining-pressure model. The analysis, including disjoining effects, follows from the pioneering work of Frumkin and Deryaguin[9−11] and has been further amplified by Sharma and Mitlin and co-workers.[22,23] On a macroscopic scale, the thin wetting layer is effectively invisible and the line-tension balance is as shown in part b of the figure. Because the analysis is local to the drop edge, only a two-dimensional problem needs to be considered. The point labeled A in Figure 3a is assumed to be sufficiently far from the substrate that its height h, when measured in units of h^*, is effectively infinite and Π is zero there. The inclination at A has become constant at the equilibrium contact angle θ_e; thus, the total pressure

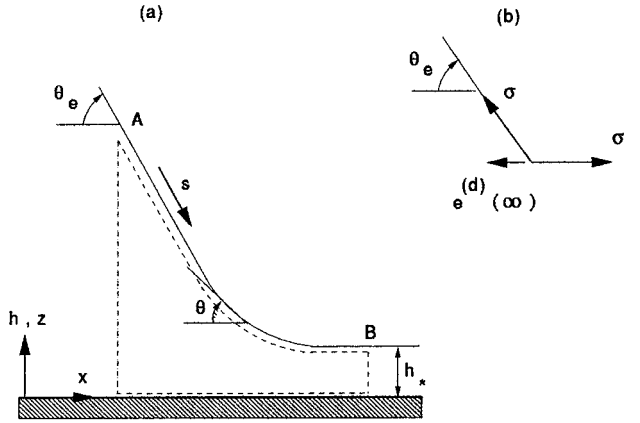

Figure 3. Contact region, at the edge of a drop, in equilibrium. A thin wetting layer of thickness h^* is used in a disjoining pressure term to specify the equilibrium contact angle θ_e: (a) Microscopic picture; (b) equivalent force balance on a macroscopic scale.

there, from eq 2.3, is zero. Similarly, at point B, on the wetting layer, the inclination θ and its rate of change along the surface are both zero, and Π is also zero there. Performing an integrated force balance in the x direction on the region enclosed by the dashed line and recognizing that the total pressure is zero on the vertical faces at A and B, we have

$$0 = \int_{h^*}^{\infty} p(h)\, \mathrm{d}h = \sigma \int_{h^*}^{\infty} \frac{\mathrm{d}\theta}{\mathrm{d}s}\, \mathrm{d}h - \int_{h^*}^{\infty} \Pi\, \mathrm{d}h$$

where s is arc length measured along the free surface. But $\mathrm{d}h/\mathrm{d}s = -\sin\theta$; thus,

$$0 = \sigma \cos\theta\big|_0^{\theta_e} - \int_{h^*}^{\infty} \Pi\, \mathrm{d}h$$

or

$$\sigma \cos\theta_e = \sigma - e^{(d)}(\infty) \tag{2.6}$$

This is the disjoining-model equivalent of the Young−Laplace eq 1.1. It is sometimes referred to as the *augmented* Young−Laplace equation.[12] Evidently

$$e^{(d)}(\infty) = \sigma + \gamma_{SL} - \gamma_{SV}$$

and $e^{(*d)}(\infty)$ is equivalent to the so-called spreading coefficient as usually employed.[25]

Using the two-term disjoining model, the constant B in eq 2.4 may be replaced in favor of θ_e using eqs 2.5 and 2.6 and

$$B = \frac{(n-1)(m-1)}{h^*(n-m)}\sigma(1-\cos\theta_e) \approx \frac{(n-1)(m-1)}{2h^*(n-m)}\sigma\theta_e^{\,2} \tag{2.7}$$

and the small-argument approximation to $\cos\theta_e$ is used for the approximate equality. Plots of disjoining pressure and disjoining energy density are given as functions of h/h^* in Figure 4. Several different exponent pairs (n,m) are compared.

(25) De Gennes, P. G. *Rev. Mod. Phys.* **1985**, *57*, 827.

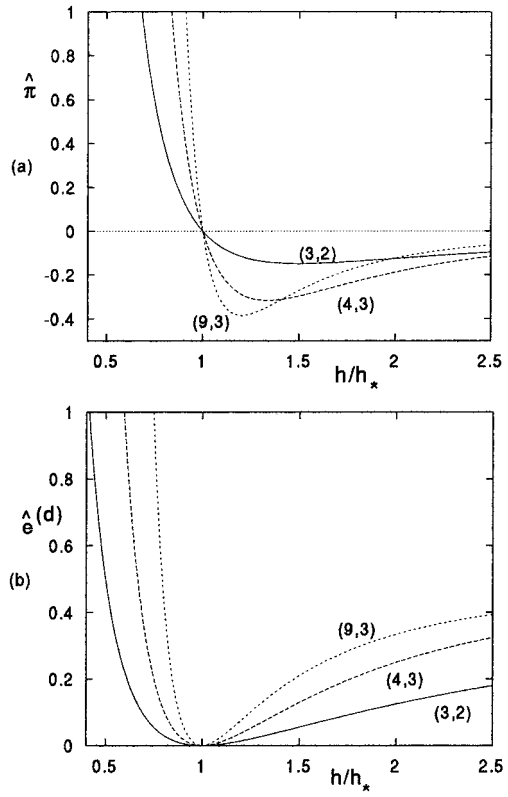

Figure 4. (a) Nondimensional disjoining pressure $\hat{\pi} = \pi h^*/(\sigma\theta_e^2)$, and (b) disjoining energy density $\hat{e}^{(d)} = e^{(d)}/(\sigma\theta_e^2)$ plotted versus dimensionless layer height h/h^* for three exponent pairs in eq 2.4.

The equilibrium contact angle is taken to be an arbitrarily prescribed function of position, and the evolution equation for flow over a heterogeneous substrate becomes

$$h_t = -\frac{\sigma}{3\mu}\nabla\cdot\left[h^3\left(\nabla\nabla^2 h + \frac{(n-1)(m-1)}{2h^*(n-m)} \times \nabla\left[\theta_e^2(x,y)\left(\frac{h^{*\,n}}{h^n} - \frac{h^{*\,m}}{h^m}\right)\right]\right)\right] + w_i(x,y,t) \quad (2.8)$$

It is possible to augmented this equation with gravity and other force terms as additional driving mechanisms.[24]

In the following we will present results using dimensionless variables. The reference state is a stationary paraboloidal drop with central height h_0 and radius R_0 lying on a flat substrate characterized by the constant equilibrium contact angle θ_{e0}. Within the small-slope assumption, the reference contact angle satisfies $\theta_{e0} \approx 2h_0/R_0$. The substrate coordinates are measured in units of R_0, while film thickness h and wetting-layer thickness h^* are measured in units of h_0. The time unit is $T^* = 3\mu R_0^4/(\sigma h_0^3)$. The evolution equation becomes, in dimensionless variables,

$$h_t = -\nabla\cdot\left[h^3\left(\nabla\nabla^2 h + \frac{(n-1)(m-1)}{2h^*(n-m)} \times \nabla\left[C\left(\frac{h^{*\,m}}{h^n} - \frac{h^{*\,m}}{h^m}\right)\right]\right)\right] + w_i(x,y,t) \quad (2.9)$$

The injection function w_i is now measured in units of h_0/T^*. All information concerning the substrate energetics is included in the function

$$C(x,y) = 4\left(\frac{\theta_e}{\theta_{e0}}\right)^2 = 4G \quad (2.10)$$

We will refer to $G(x,y)$ as the wettability.

2.1. Global Energetics. Each pressure component on the right of eq 2.3 may be identified with an integrated energy component. The free-surface energy is proportional to the area of the liquid surface and is given by

$$E_1 = E^{(\sigma)} = \sigma\int\int\left(\frac{1}{\cos\gamma} - 1\right) dA \quad (2.11)$$

where A is the total area of the substrate and γ is the angle between the normal to the surface and the normal to the substrate. Over portions of the substrate where only the thin, flat disjoining layer of thickness h^* is present, there is no contribution to E_1. With the small-slope assumption, eq 2.11 becomes

$$E_1 = E^{(\sigma)} \approx \frac{\sigma}{2}\int\int \nabla h\cdot\nabla h\, dA \quad (2.12)$$

The total disjoining energy is

$$E_2 = E^{(d)} = \int\int e^{(d)}\, dA = \frac{\sigma}{2}\int\int\theta_e^2\left[1 + \frac{m-1}{n-m}\left(\frac{h^*}{h}\right)^{n-1} - \frac{n-1}{n-m}\left(\frac{h^*}{h}\right)^{m-1}\right] dA \quad (2.13)$$

It may be verified that the integrand is zero when $h = h^*$. For $(n,m) = (3,2)$, which is the set of exponents used in this report, eq 2.13 takes the simpler form

$$E_2 = E^{(d)} = \int\int e^{(d)}\, dA = \frac{\sigma}{2}\int\int\theta_e^2\left(1 - \frac{h^*}{h}\right)^2 dA \quad (2.14)$$

Using the reference quantities introduced above, the unit of energy is σh_0^2, and the energy components are rewritten, in dimensionless form, as

$$E_1 = \frac{1}{2}\int\int \nabla h\cdot\nabla h\, dA \quad (2.12a)$$

$$E_2 = \frac{1}{2}\int\int C(x,y)\left[1 + \frac{m-1}{n-m}\left(\frac{h^*}{h}\right)^{n-1} - \frac{n-1}{n-m}\left(\frac{h^*}{h}\right)^{m-1}\right] dA \quad (2.13a)$$

The global energy change equation is now shown to be

$$\dot{E}^{(\mu)} = -(\dot{E}_1 + \dot{E}_2) + \dot{W} \quad (2.15)$$

which is the statement that the rate of viscous working is equal to the rate of decrease of the stored, or potential, energy components plus the rate of working on the system. The left side is the rate of viscous dissipation over the entire substrate

$$\dot{E}^{(\mu)} = -\int\int\mathbf{Q}\cdot\nabla p\, dA = \int\int p\nabla\cdot\mathbf{Q}\, dA = -\int\int p(h_t - w_i)\, dA \quad (2.16)$$

using eq 2.1. The divergence theorem was also used here, and we require, for example, that either p or the normal component of areal flux $Q\cdot n$ is zero at each point on the substrate boundary.

The integral in eq 2.16 can be expressed as the sum of three terms, corresponding to the right side of eq 2.15. The first of these is

$$-\dot{E}_1 = \sigma\int\int h_t\nabla^2 h \, dA = \sigma\int\int[\nabla\cdot(h_t\nabla h) - \nabla h_t\cdot\nabla h] \, dA$$

Here, again using the divergence theorem and taking $\nabla h\cdot n = 0$ on the edges of the domain to eliminate the first term on the right, we obtain

$$-\dot{E}_1 = -\frac{\sigma}{2}\frac{d}{dt}\int\int\nabla h\cdot\nabla h \, dA = -\frac{dE^{(\sigma)}}{dt} \quad (2.17)$$

Similarly, the disjoining energy term becomes

$$-\dot{E}_2 = \int\int\Pi h_t \, dA = -\int\int\frac{de^{(d)}}{dh} h_t \, dA = -\frac{d}{dt}\int\int e^{(d)} \, dA = -\frac{dE^{(d)}}{dt} \quad (2.18)$$

where $E^{(d)}$ is given for general values of (n,m) in eq 2.13. Finally

$$\dot{W} = \int\int p w_i \, dA \quad (2.19)$$

may be recognized as the rate of working on the system by means of the injection. For the cyclical motion treated below in section 4, the drop shape returns to its original configuration and there is no change, over a cycle, in E_1 or E_2. In that case the total viscous work done is the time integral of $\dot{W}$ or

$$\oint p \, dV$$

where V is drop volume, $dV = w_i \, dA$, and the special integral sign denotes a full cycle.

2.2. Numerical Techniques and Computational Issues. Equation 2.9 can be solved using finite-difference methods. It has the character of a higher-order diffusion equation and may be solved by marching in time. Equations of this type can be treated by explicit techniques, as was done by us in early work.[26] Much more efficient methods can be constructed, however. The stability requirement for an explicit method is quite severe; it is easily shown, for the model equation

$$h_t = -h_{xxxx}$$

that the maximum permissible time step for stability Δt must be no larger than order Δ^4, where Δ is the space step or mesh size. Thus the computational requirement quickly becomes more severe as the mesh size becomes small. We have found that Δ must be comparable in size to the wetting-layer thickness h^*, in dimensionless units, to maintain accuracy in the "contact region" where the macroscopic drop meets the wetting layer.

For the two-dimensional problems treated here, numerical solutions use finite difference methods and an alternating-direction-implicit (ADI) technique is implemented. Developed originally for second-order elliptic and parabolic systems,[27] the ADI technique uses alternating sweeps in each direction and only a banded system of equations needs to be solved to update the discrete set of $h_{i,j}$ values in a row or column. A version of the ADI technique called "time-splitting" has been applied to higher-order elliptic problems by Yanenko;[28] similarly another variant, due to Conte and Dames,[29] employs a predictor-corrector approach. We have used adaptations of both techniques, and they have similar performance. They each produce a high degree of stability; maximum permissible time steps can be as much as a factor of 10^5 larger than the characteristic maximum step for stability for the explicit method. For the spatially fourth-order system eq 2.9, pentadiagonal systems need to be solved to update each row or column. Apparent contact lines are captured by the method, and their motion appears as part of the evolving solution. There is no need to track or fit their positions. This benefit is not without cost, however; the computation is also performed over portions of the domain where only the thin, stagnant wetting layer is present. Nonlinear prefactors in eq 2.9 are evaluated at the old time level. The method may be made second-order-accurate in time by use of a predictor−corrector technique. Alternatively, it has been found that an adaptive time-stepping procedure, where the time step is adjusted dynamically on the basis of a preset maximum permissible change in any h value, greatly increases computational efficiency. Temporal convergence can be verified by reducing the allowed maximum change in h. Further details of the unsteady simulation methods employed here are given by Moriarty and Schwartz[30] for axisymmetrical cases and by Weidner et al.,[31] where a two-dimensional problem is solved and an ADI method is implemented.

Here the standard discretization and parameter values are $\Delta = h^* = 0.02$ for the spontaneous spreading calculations of section 3 and $(n,m) = (3,2)$. As explained in the Appendix, the isolated square defect pattern shown in Figure 2a requires specification of three lengths: the pattern wavelength λ, the defect size w, and a length d that characterizes the small length scale over which the wettability changes on the edges of each patch occur. A cubic polynomial is used over the smoothing length $2d$, so that the wetting function is continuously differentiable, as required by the field equation. The final input parameter is the minimum value G_{min} of the wettability $G(x,y)$. For $G_{min} = 1$, the substrate is uniform. As G_{min} is reduced, the contact angle on the patches increases as the field contact angle is reduced.

The cyclical calculations of section 4 used a finer mesh $\Delta = 0.01$ and $h^* = 0.01$ or 0.02. Since the calculation time is nominally proportional to the number of mesh points, these cases were more time-consuming. Calculations were made using the isolated square pattern as well as the checkerboard pattern of Figure 2b in order to discern the effect of the wettability pattern. The formulas for generating the checkerboard pattern are also given in the Appendix.

The numerical codes used to solve the evolution equation were written in the Fortran language. Runs were made on a workstation with a Pentium Pro 200 processor using Linux, a public-domain Unix operating system. Graphical output of evolving drop shapes can be stored and the results later displayed sequentially as a "movie." Run

(26) Schwartz, L. W. *Phys. of Fluids* **1989**, *A1*, 443.
(27) Peaceman, D. W.; Rachford, H. H. *SIAM J.* **1955**, *3*, 28.
(28) Yanenko, N. N. *The Method of Fractional Steps*; Springer-Verlag: New York, 1971.
(29) Conte, S. D.; Dames, R. T. *Math. Tables Aids Comput.* **1958**, *12*, 198.
(30) Moriarty, J. A.; Schwartz, L. W. *J. Colloid Interface Sci.* **1993**, *161*, 335−342.
(31) Weidner, D. E.; Schwartz, L. W.; Eres, M. H. *J. Colloid Interface Sci.* **1997**, *187*, 243.

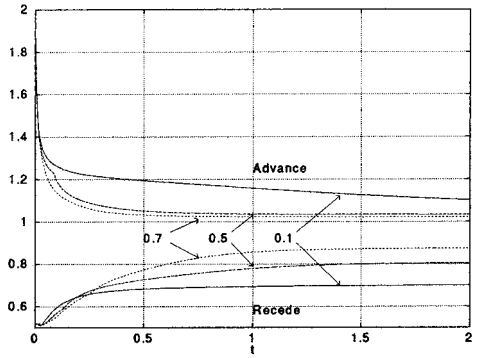

Figure 5. Central drop height versus time for substrates with large wettability contrast. Curves are labeled with the minimum value of wettability G_{min}. Different limiting values in advance and recede indicate contact angle hysteresis.

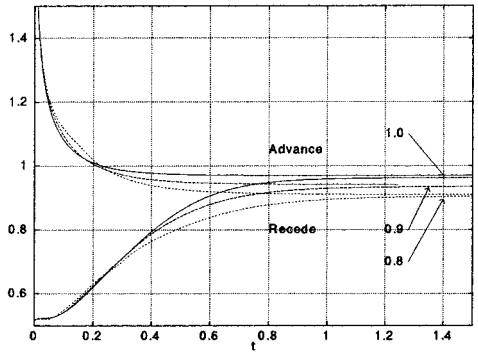

Figure 6. Central drop height versus time for substrates with small wettability contrast. Curves are labeled with the minimum value of wettability. The curves labled 1.0 are for a substrate of uniform energy. Each set of curves ultimately meets, indicating lack of hysteresis.

times varied from a few minutes for coarse-mesh cases to more than 24 h for fine meshes when the wettability contrast is relatively large.

3. Simulation of Contact Angle Hysteresis in Spontaneous Spreading

We consider a droplet on a heterogeneous substrate composed of a uniform field upon which a square pattern of "grease," that is, high-contact-angle material, has been superimposed. The contact-angle variation is given by specifying the wettability function $G(x,y)$, from eq 2.10, which is proportional to the square of the local equilibrium contact angle. The particular pattern used in this section has a wavelength λ equal to $0.4R_0$, where R_0 is the nominal drop radius, that is, the radius of a static drop if the substrate was uniform at the area-average wettability. The size of each grease patch is $0.1R_0$. The pattern is shown in Figure 2a. The smoothing length at the patch boundaries is given by $d/\lambda = 0.05$. A variable is the wettability contrast, that is, the ratio of the wettabilities on the grease patches and the surrounding field. Values of G_{min} used here range from 0.1 to 1, corresponding to equilibrium contact angle ratios $\theta_{e,max}/\theta_{e,min}$ ranging from 12.04 down to 1. Many of the graphical results are for $G_{min} = 0.5$; the contact-angle ratio for this value is 4.12. For all cases considered, the average value of G is the same, that is,

$$\frac{1}{A}\int\int G(x,y)\,\mathrm{d}A = 1 \qquad (3.1)$$

where A is the substrate area.

Figures 5 and 6 show drop central height versus time over a range of values of G_{min}. The starting profiles, at $t = 0$, are given by

$$h(r,0) = \max[h^* + h_{c,0}(1 - h_{c,0}r^2), h^*] \qquad (3.2)$$

corresponding to a paraboloidal drop superposed upon a thin wetting layer of thickness h^*. The figures show advancing cases, where the initial central height is $h_{c,0} = 2$, and receding cases with $h_{c,0} = 0.5$. All calculations are performed for $^1/_4$ of a quandrant-symmetric drop. Since the volume of the reference paraboloidal drop is $(^1/_2)\pi h_0 R_0^2$, the liquid volume for a quarter-drop, above the wetting layer, is $\pi/8$ in dimensionless units. As time proceeds, the drops move toward the nominal equilibrium position corresponding to central height $h(0,t) \approx 1$. The actual final positions depend on the strength of the wettability pattern, characterized by the value of G_{min}. The calculations were allowed to proceed until the drops ceased to move. For small wettability contrast, shown in Figure 6, the advancing and receding cases converged to the same profile for each value of G_{min}. The curves for $G_{min} = 1$ are the uniform substrate cases. Also in Figure 6 are curves for $G_{min} = 0.9$ and 0.8. In these cases as well, the advancing and receding drops ultimately find the same stable profile. These stable profiles avoid the high-contact-angle patches. Since the area-average wettability is the same for all cases, as G_{min} is reduced, the contact angle on the surrounding field also goes down. This is the reason the final drop radii increase somewhat, and the central height is reduced, as G_{min} is decreased. Figure 5, on the other hand, for larger wettability contrast, shows that the advancing and receding drops do not stabilize in the same positions. The difference in the final values of central height also reflects differences in average drop radius or effective contact angle. This difference tends to increase somewhat as G_{min} is reduced. The principal cause is the inability of the drop to find a way of passing the stronger wettability defects. The result, when the wettability contrast is sufficiently strong, that different statically stable final positions are achieved is the numerical demonstration of contact-angle hysteresis. For this particular substrate pattern, the critical value of G_{min} for CAH to disappear is about 0.75, corresponding to a contact-angle ratio of about 2.5 using eq A2 in the Appendix.

Figure 7 shows contour plots of the final positions for the advancing and receding (one-quarter) droplets when $G_{min} = 0.5$. Also shown is the wettability pattern. The drop contours are drawn for $h = 0.026$ and 0.1. For the advancing case the contour $h = 1$ is also shown. Notice how, in advance, the drop margins are held up against the pattern. In the recede case, the margins are also held up, in this case against the next "circle" of defects. For this value of G_{min}, the contact angle on the field is lower than the average value by a factor of $G_{min}^{1/2} \approx 0.707$. The corresponding equilibrium radius, using the field value of contact angle is thus larger than the nominal radius by a factor of $G_{min}^{-1/2} = 1.122$. The drop is seen to be "resting" slightly against the defect in the (2,2) position, even though this defect lies outside the nominal unit-radius circle. Three-dimensional pictures of the two stable droplets are shown in Figure 8. Indentations at the drop margins are apparent, more so for the advancing droplet, where the pinning is stronger. The wetting layer thickness used in the simulations, $h^* = 0.02$, is also visible in this figure. Because h^* is taken to be constant over the entire substrate, values of h on the thin wetting film are virtually insensitive to the local contact angle. The final central heights of the two drops are $h_a = 1.04$ and $h_r = 0.80$.

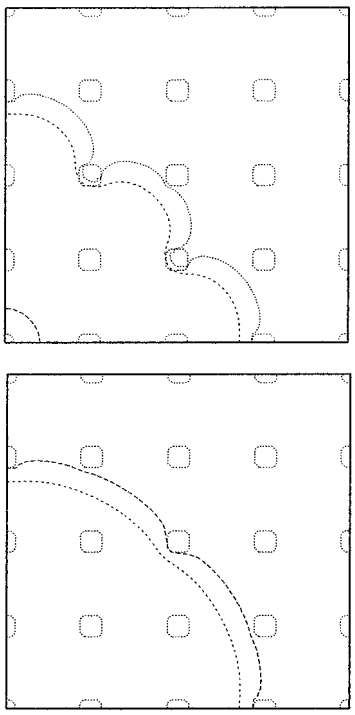

Figure 7. Contour plots of final static shapes for advanced (top) and receded (bottom) drops for $G_{min} = 0.5$ in spontaneous motion. The wettability pattern is also shown. The difference between the two cases is a measure of contact angle hysteresis.

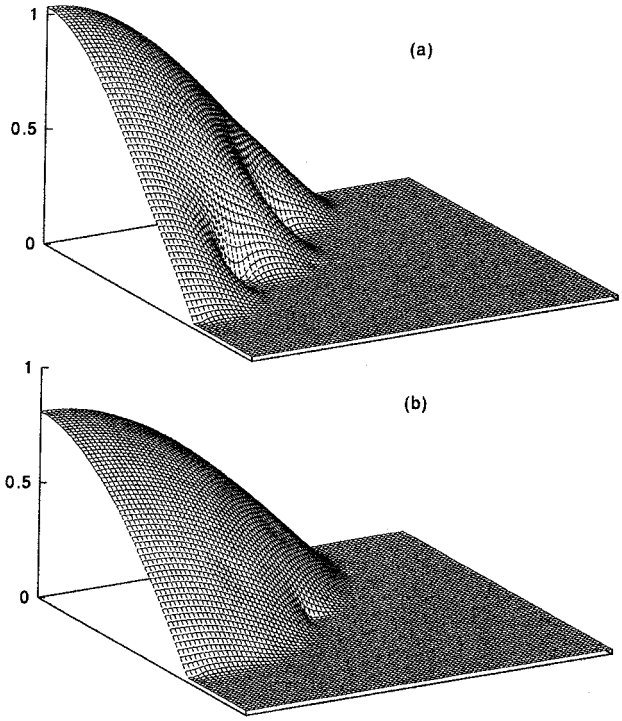

Figure 8. Wire cage pictures of drops corresponding to the contour plots in Figure 7; static advanced (a) and receded (b) drops for $G_{min} = 0.5$.

Because the volumes of the two drops are the same, the average or effective contact angle ratio is

$$\frac{\theta_a}{\theta_r} = \left(\frac{h_a}{h_r}\right)^{1/2} \tag{3.3}$$

which, in this case, is 1.14.

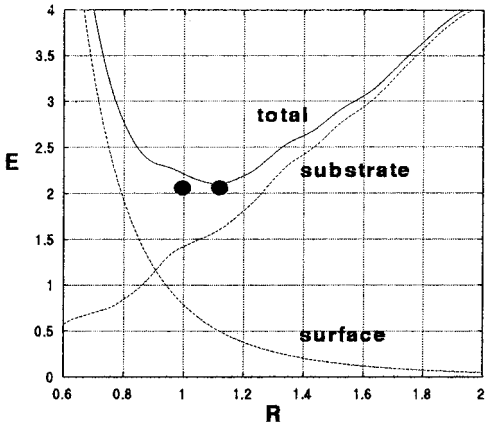

Figure 9. Plot of energy E versus drop radius R using a simple quasi-static theory. The total energy (solid line) is composed of two components (dashed lines). Here $G_{min} = 0.5$. According to the simple theory, there is only one energy minimum, and hence no hysteresis. The time-dependent theory predicts two different stable positions shown by the dots.

Figure 9 compares the configuration energies for assumed paraboloidal drops with the minimum energy positions found by the numerical algorithm for $G_{min} = 0.5$. The simple theory used for calculating the curves in the figure assumes the drops are represented by eq 3.2; the independent variable is taken as the normalized radius $R = (h(0) - h^*)^{-1/2}$, where $h(0)$ is the center height of the paraboloid. The decreasing curve in the figure is the dimensionless surface energy

$$E^{(\sigma)} = {}^1/_2 \int\int \nabla h \cdot \nabla h \, dA = \frac{\pi}{4} \int_0^R h_r{}^2 r \, dr = \frac{\pi}{4 R^4} \tag{3.4}$$

and A is the area of the quarter-circle of radius R. The undulating increasing function is the substrate energy $E^{(d)}$, calculated from eq 2.13a by integrating the actual pattern over the quarter-circle. The total energy retains the undulating character that it inherits from $E^{(d)}$. For $G_{min} = 0.5$, the amplitude of the undulations is not sufficient to produce a second local minimum in the total energy curve. For comparison, the energies for the two stable shapes, as calculated by the time-dependent program and shown in Figures 7 and 8, are shown here as large dots. The radii values for these two points use the actual center heights found by the calculation. The single energy minimum predicted by the simple theory is close to the calculated value for the receded case. The dimensionless total energy for this case is $E = 2.065$ for an equivalent radius of $R = 1.125$. The other calculated stable position is found by the advancing drop and has an energy $E = 2.064$ at $R = 0.994$. The two calculated stable positions are quite distinct; since their total energies are virtually the same, however, it is not possible for one to evolve to the other, even over a long time period, since no excess stored energy is available to overcome viscous dissipation. The simple theory used here, and its use in predicting contact angle hysteresis by looking for multiple stable energy minima, is modeled after the early work of Johnson and Dettre[2] and Neumann and Good,[3] who first calculated the hysteretic range assuming perfectly two-dimensional or axisymmetric geometries. Because the drop can realize lower total energy by avoiding patches of contamination, as for the recently advanced static picture in Figure 7a, other stable positions, that are not predicted by the simple theory, are possible. Thus the simple theory can underpredict the amount of hysteresis over complex patterns of contamination. This was rec-

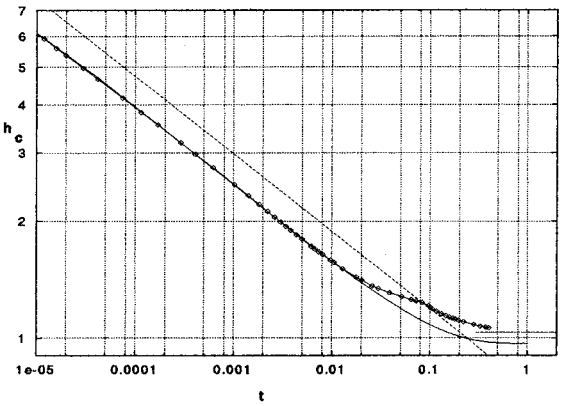

Figure 10. Drop central height h_c versus time, showing the similarity range for axisymmetric spreading. The initial drop height is 10. The straight line on this log−log plot is $h_c = 0.75t^{1/5}$, which matches experiments. The solid curve is the calculated behavior for finite contact angle on a uniform substrate, while the lines−points curve is calculated for the square wettability pattern with $G_{min} = 0.5$. The large-time height asymptote is also shown.

ognized in our earlier quasi-static analyses,[5,6] where contact-line shapes were calculated by variational methods. Other calculations made with the simple model indicate that G_{min} must be smaller than about 0.1 for the total energy curve, as in Figure 9, to have a second minimum.

Figure 10 is similar to Figures 5 and 6 in that it shows the variation of the drop central height $h(0,t)$ versus time. However here the initial paraboloidal drop shape is very much steeper; for the calculated results shown in Figure 10, the initial central height $h(0,0) = 10$. Log scales are used to demonstrate power-law behavior as the droplet expands. A second objective for the calculations shown in Figure 10 is to determine a time-scale correction that must be applied to the present calculation because the wetting-layer thickness used is overly large.

Using a lubrication-theory model for axisymmetric droplet expansion on a perfectly wetting substrate, Tanner[15] predicted that the droplet central height should decrease as a function of time to the $-1/5$ power. He also confirmed this prediction experimentally. The straight line shown in the figure fits the equation

$$h_c = h(0,t) = \frac{K}{t^{1/5}} \tag{3.5}$$

with $K = 0.75$, which is representative of spreading rates for water drops on high-energy substrates. Experiments of Lelah and Marmur[17] examined the spreading of water drops on clean glass and found that the droplet area A increased according to the law

$$A = CV^{3/5}t^{1/5} \tag{3.6}$$

where V is droplet volume and t is dimensional time. C is a dimensional constant with units of speed to the one-fifth power. Values of C, obtained from curve fits to the data, varied from 11 to about 15 in cgs units, with the larger values obtained when the relative humidity was high. It can be shown that the constants C and K satisfy

$$K = \frac{2}{C}\left(\frac{\pi}{2}\right)^{5/2}\left(\frac{\sigma}{3\mu}\right)^{1/5} \tag{3.7}$$

Using the values for water, $\mu = 0.01$ P and $\sigma = 72$ dyn/cm, the value $C = 15$ corresponds to $K = 0.75$. Previous calculations, using an axisymmetric form of the present algorithm that allows much larger spatial resolution,[24] produced spreading with $K = 0.75$ when $h^*/h_0 = 5 \times 10^{-4}$. Using the present program, with $h^*/h_0 = 0.02$, yields the results shown in Figure 10 by the solid curve and the lines−points curve. In the straight-line range, they are closely approximated with K taken as 0.62. Thus, as h^* is varied, spreading follows the same power law, but the constant K in eq 3.5 is weakly dependent on the actual value of h^*.

Spreading speeds must be compared at the same drop position rather than at the same time. Differentiating eq 3.5 with respect to time, one obtains

$$\frac{\partial h_c}{\partial t} = -\frac{K}{5t^{6/5}} = -\frac{h_c^6}{5K^5} \tag{3.8}$$

Since the droplet expansion rate $\partial R/\partial t$ is proportional to $-\partial h_c/\partial t$, the spreading speed is proportional to K^{-5}. Using the calculated results above, for example, and changing h^* from 2×10^{-2} to 5×10^{-4} reduce the spreading rate by a factor of about 2.6. This is a correction factor that should be applied to the time scale due to our present inability to run a sufficiently fine spatial mesh to resolve very thin wetting-layer thicknesses h^* in multidimensional problems. Using values for water and assuming a drop with central height $h_c = 0.02$ cm and radius $R = 0.5$ cm, the unit of time is $T^* = 3.25$ s. Using currently feasible values of h^*, we estimate that the time-scale correction should increase T^* by a factor of between 2 and 4. This will of course depend on the nature of the spreading liquid and the experimental conditions such as the relative humidity. This is consistent with local asymptotic analyses of spreading; those results[15,16] indicate the speed of advance should scale as $1/\log(h_1/h^*)$, where h_1 is a macroscopic measure of droplet thickness.

The calculated results shown in Figure 10 are found using the present program with finite equilibrium contact angles. It is significant that they follow the same power law as for spreading on perfectly wetting substrates, when they are far from the equilibrium value $h_c \approx 1$. This is consistent with the experimental observations of Zosel,[32] who noted that the nature of the substrate only appeared to influence spreading rates quite close to equilibrium. It is also noteworthy that the results for the nonuniform substrate (lines-with-points) are essentially identical to those for the uniform-substrate case (solid curve) until the drop nears its final position.

Figure 11 illustrates an interesting transient effect during the receding calculation for $G_{min} = 0.5$. At an early time in the calculation, before the drop has contracted an appreciable amount, dry patches appear near the drop periphery. These dry areas appear entirely within the receding contact line. They are caused by high values of disjoining pressure immediately over the patches of contamination in the relatively thin border region of the drop. This *dewetting instability* is absent in the advancing calculations, since the high interior capillary pressure makes the drop expand too rapidly for interior dry patches to form. The receding contact line ultimately passes the interior dry patches via a slow drainage process, and the final receding drop configuration is the one shown in Figure 8b.

Figure 12 is a plot of total energy versus time for the advancing and receding cases with $G_{min} = 0.5$. Both curves ultimately reach the values $E \approx 2.06$, but the receding

(32) Zosel, A. *Colloid Polym. Sci.* **1993**, *271*, 680.

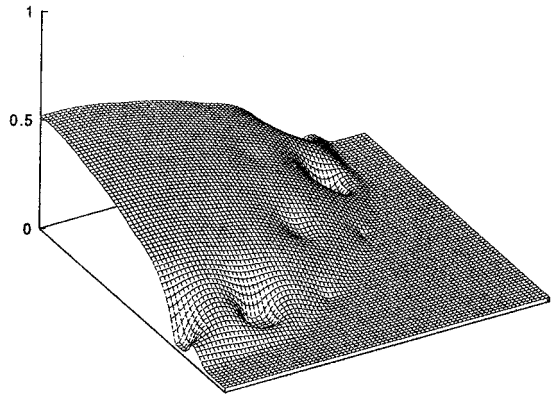

Figure 11. Frame during recede at $t = 0.014$ for $G_{min} = 0.5$. A dewetting instability leads to interior dry patches near the receding periphery. This is a transient effect, and the drop copntinues to recede until the final configuration, shown in Figure 8b, is attained.

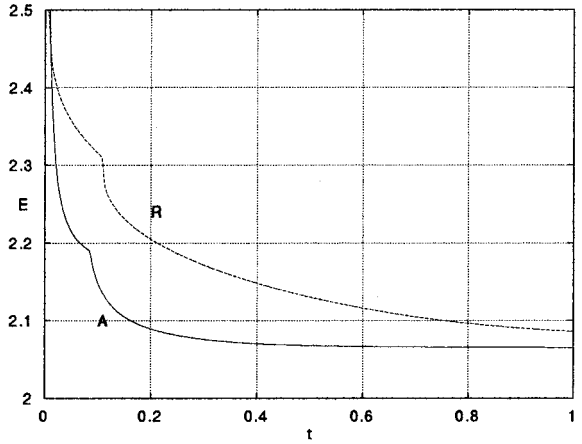

Figure 12. Total energy versus time: a comparison of the advancing (A) and receding (R) cases; $G_{min} = 0.5$. Steep-slope regions correspond to rapid events as the meniscii pass patches of high-contact-angle material.

case proceeds at a much slower rate, due primarily to the development of dry patches as noted above. Also visible, on each curve, are "jumping events" that correspond to the drop being temporarily hung up on, and finally breaking free of, the patches of contamination.

4. Simulation of Cyclical Motions on Contaminated Surfaces

The previous section dealt with spontaneous motions in that the only driving mechanism is the energy stored in the free-surface shape and the substrate wettability pattern. In each case, the motion ultimately stops when the drop has found a stable position. Here we treat a class of forced motions where a sessile drop is made to spread by slowly increasing its volume by injection, as with a syringe. A full cycle is simulated by first injecting liquid into the drop and then withdrawing the liquid until the drop returns to its original shape and position. The notional experiment is shown schematically in Figure 13. This is the geometry analyzed in this section. For definiteness, the injection is taken to be through the substrate, so that the liquid free surface remains smooth. Again we will calculate motions on one-quarter of a quandrant-symmetric drop. We note, however, that syringe injection through the free surface may be more likely to ensure that the drop remains centered in an actual experiment.

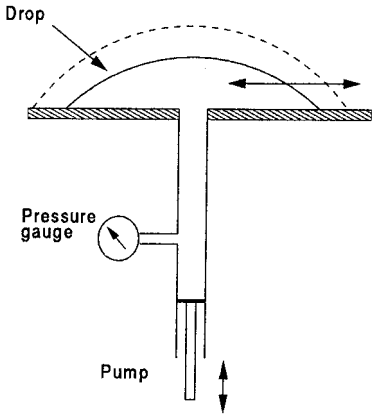

Figure 13. Schematic diagram of a notional experiment to investigate energy dissipation in a cyclic motion of a drop. The pump piston slowly moves in and out while the pressure is being monitored in order to calculate the work done on, or by, the system.

The governing time-dependent lubrication equation (eq 2.1) now includes the injection term $w_i(x,y,t)$. The drop is assumed to be centered over the syringe and the injection profile is taken to be axisymmetric,

$$w_i(r,t) = \frac{Q}{2t_c R_i^2} e^{-r^2/R_i^2} \tag{4.1}$$

where $r = (x^2 + y^2)^{1/2}$. Here R_i is a measure of the injection radius. All results below use $R_i = 0.4\,R_0$. t_c may be called the characteristic time for injection. Starting with a paraboloid of normalized central height and radius both equal to 1, if w_i is given by eq 4.1 and $Q = 1$, then the volume will be doubled over the time interval $\Delta t = t_c$. Starting from an initial paraboloidal shape, a drop is made to expand and then contract according to the following schedule:

$$0 < t < t_c/2 \quad Q = 0$$

$$t_c/2 < t < {}^3/_2 t_c \quad Q = 1$$

$${}^3/_2 t_c < t < 2\,t_c \quad Q = 0$$

$$2t_c < t < 3t_c \quad Q = -1$$

The total period is $3t_c$ and consists of a relaxation period, followed by a period of constant injection at unit injection rate, a second relaxation period, and a final withdrawal period also at unit injection rate. For most of the results in this section the substrate wettability pattern is taken to be a "checkerboard" rather than the square pattern of discrete high-contact-angle spots. The checkerboard function is doubly periodic and is given by

$$G(x,y) = 1 + a f_1(x)\, f_1(y) \tag{A.3}$$

where a is the input amplitude. For the results given below, a will be 0.5 or, for a homogeneous substrate, $a = 0$. The function f_1 is a periodic power-law that varies between $+1$ and -1 and whose specific form is given in the Appendix. The power-law exponent used here is 6; this produces a wettability function that is almost a square wave, but the discontinuities at patch boundaries are smoothed.

A contour plot for a statically stable drop on the checkerboard is shown in Figure 14. The contours of

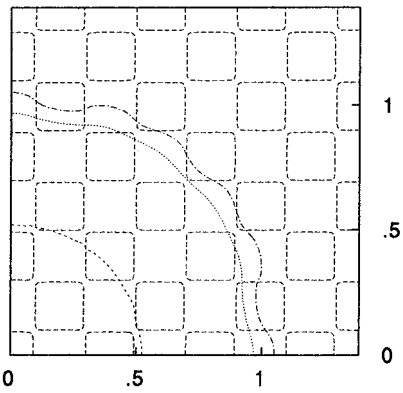

Figure 14. Contour plot of a statically stable drop on the checkerboard pattern. The ratio G_{max}/G_{min} is 3. The wetting layer thickness is $h^* = 0.01h_0$. Contour levels shown are 0.013, 0.1, and 0.7. On a uniform substrate with the same average wettability, the drop central height $h(0,0)/h_0$ and radius R/R_0 are each about equal to 1. The checkerboard is drawn so that the high-contact-angle regions are enclosed.

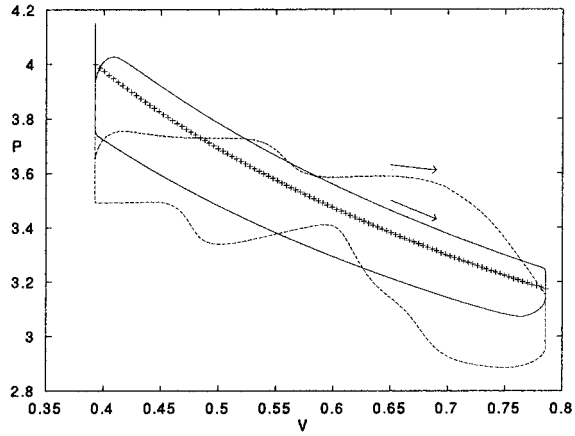

Figure 15. Dimensionless pressure P versus volume V showing hysteresis loops in cyclical motion. The cycle time $t_c = 5$. The solid line is for a uniform substrate, and the dashed line is for a checkerboard wettability pattern. The ratio G_{max}/G_{min} is 3. The symbol curve is for the nondissipative quasi-static theory with the equation $P = 2\pi^{1/3}V^{-1/3}$. Arrows show the direction of motion around the loops. The energy dissipation for the full cycle, corresponding to the enclosed area, is 0.106 for the uniform substrate and 0.143 for the checkerboard.

surface wettability $G(x,y)$ are drawn for a value of G slightly greater than the average value, so that the high-contact-angle regions appear enclosed. The ratio of contact angles on the checkerboard elements is $[(1 + a)/(1 - a)]^{1/2} = \sqrt{3}$. The drop edge contours are seen to deform to avoid a portion of the high-contact-angle material. The deformation is much less, however, than that for the stronger isolated-spot pattern of Figure 7a, for example.

Figure 15 is a pressure P versus volume V plot for an injection-withdrawal cycle using $t_c = 5$. The rate of injection work, from eq 2.19, is

$$\frac{dW}{dt} = \int\int p w_i \, dA = \frac{Q}{2t_c R_i^2}\int\int p(x,y) e^{-r^2/R_i^2} \, dA \qquad (4.2)$$

while the rate of volume increase is

$$\frac{dV}{dt} = \int\int w_i \, dA = \frac{\pi}{8}\frac{Q}{t_c} \qquad (4.3)$$

The pressure p in eq 4.2 includes capillary and disjoining components as in eq 2.3. Since p is effectively zero in the wetting layer outside the drop, the area integral in eq 4.2 may be taken over the entire substrate. An average pressure P is then

$$P = \frac{dW}{dV} = \frac{4}{\pi R_i^2}\int\int p e^{-r^2/R_i^2} \, dA \qquad (4.4)$$

P will be the average pressure at the piston face in Figure 13, provided the motion is sufficiently slow so that viscous work in the syringe, between the piston and the drop opening, can be neglected. Note that P is defined in all phases of the motion including the relaxation periods. In general, positive work is done on the system during the injection phase, while the system does work on the piston during withdrawal. No work is done during the relaxation periods. In these periods, the drop seeks an equilibrium configuration as some of the stored energy is dissipated by viscosity according to eq 2.15. Since the drop is allowed to return to its equilibrium shape after a full cycle, the net work done is equal to the total energy consumed in the motion. This work corresponds to the enclosed area for each closed loop in Figure 15, in accordance with the usual definition of hysteresis in mechanical systems.

Three different loops are shown in Figure 15. The range of V is from $\pi/8$, the original volume of the quarter-drop in dimensionless units, up to twice that value. Motion on a homogeneous substrate with the same average wettability, shown as the solid-line loop, is compared with motion on the checkerboard, denoted by the dashed loop. The arrows indicate the direction of motion on each of the loops. The checkerboard loop shows significant irregularity, corresponding to the various contact-line distortions during the cycle. Energy is temporarily stored in these distortions and then is quickly released as the injection or withdrawal proceeds. The enclosed area for the homogeneous loop is 0.106; this is the dissipated energy measured in units of σh_0^2. For the checkerboard, the calculated dissipation is 0.143. The difference may be considered to be the additional work done due to the distortion caused by the pattern of wettability.

Also shown in Figure 15 is a single curve denoted by symbols. This is the result of a simple quasi-static theory appropriate to a very slow cycle on a homogeneous substrate. The drop is taken to be a paraboloid that always meets the substrate at the equilibrium contact angle $\approx 2h_0/R_0$ as the volume is varied. The pressure within the drop is independent of position and is equal to $4h_c/R^2$, measured in units of $\sigma h_0/R_0^2$ and using the small-slope approximation. The resultant dimensionless quasi-static pressure–volume relation is

$$P = \frac{2\pi^{1/3}}{V^{1/3}} \qquad (4.5)$$

The dynamic loop for the homogeneous substrate is seem to form an envelope around the quasi-static curve, indicating, for example, that the advancing contact angle exceeds the equilibrium value, while the contact angle in recede is smaller than the equilibrium value. Both sides of the loop approximately follow the $V^{-1/3}$ law, implying that the dynamic angles are essentially constant during the appropriate phases. Since the speed of the droplet edges is not constant during either advance or recede (in fact the "contact-line" speed is proportional to $V^{-2/3}$), the often-used *ansatz* that the dynamic contact angle is a unique function of speed is not supported by these results.

Figure 16 is the pressure–volume plot, for the same substrates, for a motion that is five times as fast. For the

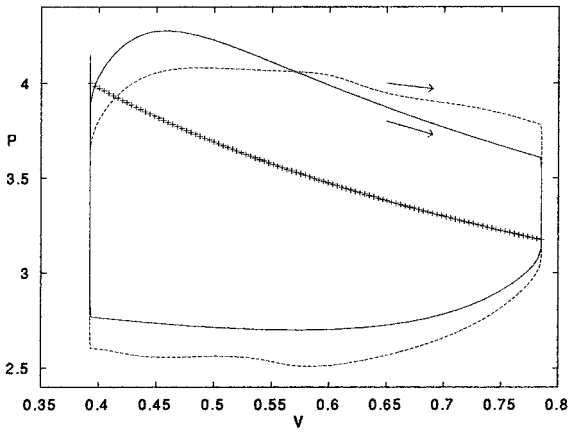

Figure 16. Dimensionless pressure P versus volume V showing hysteresis loops in cyclical motion. The cycle time $t_c = 1$. This motion is 5 times as fast as the one in the previous figure. The solid line is for a uniform substrate, and the dashed line is for a checkerboard wettability pattern. The ratio G_{max}/G_{min} is 3. The symbol curve is the same as that in the previous figure. Arrows show the direction of motion around the loops. The energy dissipation for the full cycle is 0.480 for the uniform substrate and 0.534 for the checkerboard.

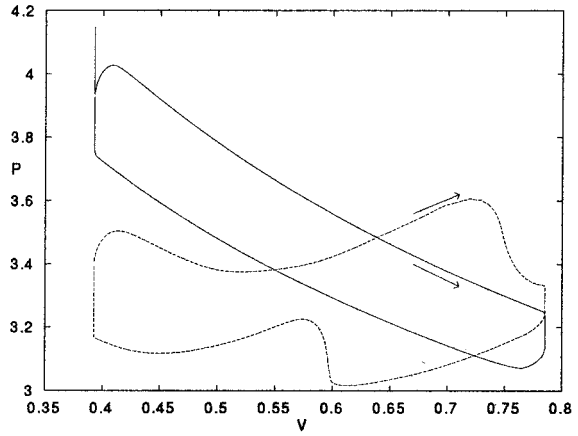

Figure 17. Dimensionless pressure P versus volume V showing hysteresis loops in cyclical motion for the isolated square pattern. The cycle time $t_c = 5$. The uniform substrate (solid) and the isolated square pattern (dashed line) with $G_{min} = 0.8$ are compared. $h^* = 0.01$, and $\Delta = 0.01$ for both. Arrows show the direction of motion around the loops. The energy dissipation for the full cycle is 0.106 for the uniform substrate and 0.131 for the isolated square pattern. While the isolated pattern is more effective for pinning the drop edges, since the wettability contrast is higher, 5 versus 3 for the checkerboard, the checkerboard is more effective for dissipating energy.

homogeneous substrate, the dissipation is 0.480, about five times as large as that for the previous slow motion. That the dissipation should be approximately proportional to the speed, in a forced motion, follows from elementary considerations; dynamic pressure differences are proportional to speed when inertial effects are negligible, as in eq 2.2. In advance the $V^{-1/3}$ law is still approximately valid, indicating that the effective advancing contact angle is almost constant. The receding pressure is more nearly constant, representing a large deviation from the quasi-static law. The calculated dissipation on the checkerboard pattern is larger than that for the homogeneous substrate; however, the additional work is only a bit larger than that for the slow cycle shown in Figure 15. The pattern-crossing undulations in the pressure are considerably reduced compared with those for the slow case. This indicates that the drop does not have enough time to deform appreciably at any given location on the pattern.

Results for another slow cycle and shown in Figure 17. The difference is that the pattern is now the isolated spots with $G_{min} = 0.8$. The corresponding ratio of contact angles is $\sqrt{5} \approx 2.236$ while, for the checkerboard of Figure 15, the contact angle ratio was $\sqrt{3} \approx 1.732$. Because the ratio is larger, stronger "pinning" can be expected as the drop margins become temporarily trapped near the edges of the grease patches. Since volume changes are proportional to time changes, either in injection or withdrawal, the large slope regions on the pressure−volume curve are indicative of "jumping" motions. By comparison with the results of section 3, it is seen that $G_{min} = 0.8$ is not small enough for contact-angle hysteresis in spontaneous motions. Thus, for slow enough motions, a closed pressure−volume loop is attained on the very first cycle. While the isolated pattern shown here is clearly more effective for pinning the drops, it actually dissipates less energy per cycle than the checkerboard. The numerical value is 0.131 compared with 0.143 in Figure 15.

5. Discussion and Conclusions

The feasibility of calculating the unsteady motion of a liquid droplet on particular patterns of wettability, using a disjoining pressure model to characterize the substrate, has been demonstrated. Calculations are performed using a stable and efficient alternating-direction-implicit algorithm. Estimates of the degree of heterogeneity required to produce contact angle hysteresis on various patterns can be made using this procedure. It is found that even when the heterogeneity is insufficient to result in multiple stable configurations, the motion can be slowed significantly by the substrate defects. We suggest, therefore, that, in the interpretation of experimental measurements of contact angle hysteresis, care must be taken to ensure that sufficient time has elapsed before the nominal steady-state angle is measured. Slow relaxation to equilibrium is especially likely for receding contact lines, as has been shown in the calculations of Figure 6. Receding contact lines lead to relatively thin liquid layers; these thin layers are susceptible to interior dewetting over substrate defects, as shown in Figure 11.

A basic issue in industrial applications is the level of cleanliness that must be maintained for successful coating. The speed of spreading motions on imperfect, that is, contaminated, surfaces is generally relevant here. The time scale required to overcome substrate defects must be compared with the characteristic time for drying of a coating. While there may be no hysteresis in a quasi-static sense for an assumed nonvolatile liquid, weak defects still impede spreading and may result in inadequate coverage in an actual dry coating.

The results of the present dynamic studies are consistent with previous quasi-static analyses of CAH in that motions cease when the system finds a local minimum of total energy. However, the very simplest static theories that assume the shape of the liquid surface to be of a simple form can fail to predict CAH when it is present. Even if system energies are calculated in detail, as in our previous work,[5,6] the necessary assumption, that the system progresses from one energy minimum to another in forced motions, may lead to incorrect results at all but the slowest possible speeds. Because the present work is a direct numerical simulation, there are no inherent restrictions on the geometry of the liquid region or the possible patterns of wettability. The quasi-static analyses are essentially theoretical methods that employ rather sophisticated geometric and variational techniques. The dynamic simulation is conceptually simpler and is easier to

implement. It makes use of computational resources that were not available when the quasi-static theories were formulated.

Forced cyclical motions on homogeneous and patterned substrates have been investigated. On a perfectly homogeneous substrate, low-speed axisymmetric motions compare well with the result of a simple quasi-static theory. For the patterned substrates, the substrate-averaged wettability is the same as that for the homogeneous case. When a pattern is used, the total energy dissipation per cycle increases. By comparing cyclical motions at different speeds, it has been demonstrated that the relative importance of the pattern increases as the speed is reduced. Isolated-spot patterns cause greater deformations of the drop and more rapid changes in the total system energy. It cannot be concluded, however, that these greater distortions lead to greater overall dissipation. Comparing the cyclical motion on two different substrate patterns, we find that the dissipation is actually greater for a pattern with a smaller wettability contrast. The more dissipative pattern is the "checkerboard" shown in Figures 2 and 14. While the wettability contrast is smaller for this pattern, it is noted that the total arc length of the wettability boundaries is larger by a factor of 4 for the checkerboard, when compared with the spot pattern. Clearly both the wettability contrast and the length of the boundaries contribute to the added dissipation caused by the pattern.

Application of a wettability pattern to the walls of vessels containing liquid is a possible strategy for controlling the position of the liquid in the microgravity environment of orbiting space vehicles. In the absence of gravity, liquid in a partially filled container can assume many different configurations. Small imposed accelerations can cause large displacements of the liquid, which is undesirable for a variety of reasons. Contact line dynamics will play an important role, either by "pinning" the location of the liquid on the wall or by dissipating the kinetic energy imparted to the liquid. The present results suggest that different wall wettability patterns may accomplish one or the other of these objectives.

The disjoining model used here has a single stable energy minimum. A thickness less than the equilibrium thickness h^* will be repelled from the substrate while a thicker layer will be attracted to it. The local shape of the energy "well" is given by its second derivative at $h = h^*$, which, using the present model, is

$$\left[\frac{\mathrm{d}^2 e^{(d)}}{\mathrm{d}h^2}\right]_{h=h^*} = \frac{\sigma\theta_e^{\,2}}{2h^{*2}}(m-1)(n-1) \qquad (5.1)$$

The choice of exponent pairs (n,m) determines the depth of the energy well; this is illustrated in Figure 4. Previous work[24,33] has shown that a choice such as (4,3) or (9,3) increases the "stiffness" of a drop, relative to that for the (3,2) pair used here. The deformation of droplet edges at wettability boundaries can be expected to be smaller than what is calculated here when the other pairs are used. Larger gradients in $e^{(d)}(h)$ require somewhat finer numerical meshes, resulting in longer computation times. This is the primary reason for the exponent choice used here. More complicated functional forms for $e^{(d)}(h)$ have also been used in static and dynamic studies.[11,18,22] The effect of this choice of function on the time-dependent dynamics of motion on mixed-wettable substrates remains to be explored. Replacement of the present disjoining law with other forms is easily done in the numerical simulation.

Wetting-line speeds in spontaneous motions are controlled by the thin equilibrium layer thickness h^*. For spreading on homogeneous substrates, spreading rates are virtually independent of the value of the static contact angle until the drop has almost stopped. In this regime the disjoining function also is unimportant. This independence has been observed experimentally[32] and confirmed by calculation.[24] The speed dependence on h^* is known to follow a logarithmic law for the homogeneous case.[15,16,25] For one-dimensional or axisymmetric problems it is possible to use realistically small values of h^* so that good agreement with experiment can be expected. Accurate simulation results require that the scaled mesh size Δ be comparable with or smaller than h^*; thus, realistic values of h^* cannot yet be used in two-dimensional simulations. The logarithmic law predicts that reducing h^* by a factor of order 10^2 to 10^3 will lead to a speed reduction factor between 2 and 4. Thus the spreading rates calculated here are expected to be larger than what will be observed experimentally.

The dependence on h^* is somewhat different for forced motions. For very slow motions one may assume that the local speed of the contact line U is directly proportional to the injection rate and thus is independent of h^*. Assume that a local force F, per unit contact-line length, drives the motion. F is balanced by the integrated shear stress on the substrate

$$\int \tau(0)\,\mathrm{d}x = 3\mu U \int \frac{\mathrm{d}x}{h} = \frac{3\mu U}{\theta_e}\int \frac{\mathrm{d}h}{h} \qquad (5.2)$$

using $\mathrm{d}h/\mathrm{d}x \approx \theta_e$, which is appropriate to the wedge-shaped contact region where most of the viscous work is done. If the limits of integration on h are h^* and some h_1, one obtains[25]

$$F = \frac{3\mu U}{\theta_e}\log\left(\frac{h_1}{h^*}\right) \qquad (5.3)$$

Here h_1 is a macroscopic drop thickness that is assumed constant as $h^* \to 0$. Identifying h_1 with the drop central height, which is approximately 1 in dimensionless units, the local rate of working FU will vary logarithmically with h^*. Equation 5.3 predicts that replacing $h^* = 0.01$ by $h^* = 0.02$ will reduce the work done per cycle by 15%. The four cases of forced motion whose results are shown in Figures 15 and 16 were rerun with $h^* = 0.02$. In each case the total work done was reduced; the reductions varied from seven to 15%.

There is a need for experimental measurements that can be compared with the calculated results. The present mathematical model employs a variety of simplifying assumptions; thus, experimental validation is required for specific features of the motions predicted. A candidate or "notional" experiment is outlined in section 4. Energy transfer to and from that system can be obtained if the injection pressures can be accurately measured. This will require pressure resolution of 1 mm of H_2O or less. Regular patterns of wettability on scales of 10−100 μm can be produced using microfabrication techniques, as employed in the electronics industry, for example. Low-power microscopy can be used to observe the droplet distortions near the moving contact lines.

Naturally occurring heterogeneous surfaces will have characteristic lengths for the inhomogeneity that can be

(33) Schwartz, L. W. *Proc. 3rd Micrograv. Fluid Phys. Conf.* **1996**, *3338*, 609.

significantly smaller than this. It will be useful to investigate to what extent the hysteretic behavior on a naturally heterogeneous surface, that must also exhibit a degree of randomness, is similar to that on a prepared patterned surface. Some aspects of randomness and its influence on hysteresis have recently been discussed by Collet et al.[34]

The principal purpose of the present work has been to demonstrate the feasibility of time-dependent simulation. Relatively few defects have been traversed by the moving boundary of the drop. It is possible, at greater computational cost, to consider more defects and defects arranged in more complicated patterns in order to more closely simulate behavior on a natural material. For relatively large drops, gravity can be included in the simulation. This has been done for a related problem[24] and can be included here without difficulty.

Acknowledgment. This work is supported by the NASA Microgravity Program, the ICI Strategic Research Fund, and the State of Delaware.

Appendix: Substrate Wettability Functions

(i) Isolated-Spot Patterns. We consider a planar substrate with a constant average wettability. A periodic square pattern of wettability with wavelength λ is generated by the following procedure. The wettability function $C(x,y)$ in eq 2.9 is given by

$$C(x,y) = 4G(x,y)$$

where

$$G(x,y) = G_{\min} + \frac{1 - G_{\min}}{w^2} f(x)\, f(y) \qquad \text{(A.1)}$$

Here $0 \le G_{\min} \le 1$ is the minimum value on the pattern, corresponding to the "clean" or high-energy areas. w is the fraction of λ occupied by the patch of contamination. The function f is a periodic piecewise smooth function of one variable consisting of constant values connected by cubic polynomials. It is given by

$$f(x) = F(x/\lambda - [x/\lambda]; w, d)$$

where the square brackets signify the "integer part" function and $F(\xi)$ is

$$\begin{aligned}
&1 && 0 \le \xi \le \xi_1 \\
&\frac{1}{2} - \frac{3}{4}\left(R_1 - \frac{{R_1}^3}{3}\right) && \xi_1 < \xi \le \xi_2 \\
&0 && \xi_2 < \xi \le 1 - \xi_2 \\
&\frac{1}{2} + \frac{3}{4}\left(R_2 - \frac{{R_2}^3}{3}\right) && 1 - \xi_2 < \xi \le 1 - \xi_1 \\
&1 && 1 - \xi_1 < \xi \le 1
\end{aligned}$$

Here we have defined the constants

$$\xi_1 = \frac{w}{2} - d, \quad \xi_2 = \frac{w}{2} + d$$

and the linear functions

$$R_1(\xi) = \frac{\xi - \frac{w}{2}}{d} \quad R_2(\xi) = \frac{\xi - 1 + \frac{w}{2}}{d}$$

The small quantity $2d < w$ is the width of the region between the two constant plateau values. d is also expressed as a fraction of λ. It is used to provide continuous derivatives for $C(x,y)$, as used in eq 2.9. Second derivatives are bounded but discontinuous where the cubic meets the constant values. It is easily verified that

$$\int_0^1 \int_0^1 G(x,y)\, dx\, dy = 1$$

thus the average value of wettability is constant, irrespective of the value of $G_{\min}$. If $G_{\max}$ is the maximum value of G on the pattern, the ratio of equilibrium contact angles is

$$\frac{\theta_{e,\max}}{\theta_{e,\min}} = \frac{1}{w}\left(\frac{1 - G_{\min}(1 - w^2)}{G^{\min}}\right)^{1/2} \qquad \text{(A.2)}$$

since $G(x,y)$ is proportional to ${\theta_e}^2$, under the small-slope approximation.

(ii) Checkerboard Patterns. The checkerboard pattern of Figure 2b is generated by

$$G(x,y) = 1 + a f_1(x)\, f_1(y) \qquad \text{(A.3)}$$

where $0 \le a \le 1$ is an input amplitude parameter. The function f_1 is odd with period λ. Let

$$\eta = x + \frac{\lambda}{4} - \left[\frac{x + 3\lambda/4}{\lambda}\right]\lambda$$

where again the square brackets signify the integer-part function. The range of η is $(-\lambda/2, \lambda/2)$. f_1 is given by

$$1 - \left(\frac{4\eta}{\lambda} - 1\right)^m \qquad \eta > 0 \qquad \text{(A.4a)}$$

and

$$-\left[1 - \left(\frac{4\eta}{\lambda} + 1\right)^m\right] \qquad \eta < 0 \qquad \text{(A.4b)}$$

It may be verified that f_1 has a continuous first derivative and a bounded, but discontinuous, second derivative at $\eta = 0$. The input parameter m is a positive even integer. Since the range of f_1 is $[-1,1]$, the maximum and minimum values of G are $G_{\max} = 1 + a$ and $G_{\min} = 1 - a$. It may be verified that the area-average wettability is also equal to 1 for the checkerboard.

LA971407T

(34) Collet, P.; De Coninck, J.; Dunlop, F.; Regnard, A. *Phys. Rev. Lett.* **1997**, *79*, 3704.